International Journal of Automotive Technology, Vol. 20, No. 5, pp. 923–932 (2019)
DOI 10.1007/s12239–019–0086–8

pISSN 1229–9138/ eISSN 1976–3832

YAW STABILITY CONTROL OF 4WD VEHICLES BASED ON MODEL PREDICTIVE TORQUE VECTORING WITH PHYSICAL CONSTRAINTS

Kwangseok Oh[1)*], Eunhyek Joa[2)], Jisoo Lee[3)], Jaemin Yun[3)] and Kyongsu Yi[2)]

[1)]Department of Mechanical Engineering, Hankyong National University, Gyeonggi 17579, Korea
[2)]School of Mechanical and Aerospace Engineering, Seoul National University, Seoul 08826, Korea
[3)]Chassis System Control Development Team, Hyundai Motor Company, 150 Hyundaiyeonguso-ro, Namyang-eup, Hwaseong-si, Gyeonggi 18280, Korea

(Received 27 June 2018; Revised 3 February 2019; Accepted 12 February 2019)

ABSTRACT–This paper describes a yaw stability control algorithm of 4WD vehicles based on model predictive torque vectoring with physical constraints. A vehicle planar model based predictive rear and all-wheel torque vectoring algorithms were developed for 4WD vehicles by considering predictive states and driver's steering wheel angle. The physical constraints applied to the model predictive control consist of three types: limitation on magnitude of tire force, change rate of tire force, and output torque of transfer case. Two types of torque vectoring algorithms, rear-wheel and all-wheel, were constructed for comparative analysis. The steady state yaw rate was derived and applied as a desired value for yaw stability of the vehicle. The algorithm was constructed in a MATLAB/Simulink environment and the performance evaluation was conducted under various test scenarios, such as step steering and double lane change, using the CarSim software. The evaluation results of the predictive torque vectoring showed sound performance based on the prediction of states and driver's steering angle.

KEY WORDS : Model predictive control, Torque vectoring, Physical constraint, Torque distribution, Yaw stability

NOMENCLATURE

$\dot{\psi}$: yaw rate, rad/s
m : vehicle mass, kg
l_f : distance between mass center and front axle, m
l_r : distance between mass center and rear axle, m
C : cornering stiffness, N/rad
δ : steering angle, rad
v : velocity, m/s
t_w : vehicle width, m
F : tire force, N
I : moment of inertia, kg m^2
N : prediction step
r_w : wheel radius, m
e : error state
u : input
w : disturbance
ω : wheel speed, rad/s

SUBSCRIPTS

x, y, z : longitudinal, lateral, and vertical
fl, fr, rl, rr : front-left, front-right, rear-left, and rear-right
ss : steady-state
des : desired
d : discretized
eq, in : equality, inequality

*Corresponding author. e-mail: oks@hknu.ac.kr

1. INTRODUCTION

Recently, the development of various vehicle technologies related to safety control, such as autonomous emergency braking system (AEBS), electronic stability control (ESC), and torque vectoring, has been accelerated by many research organizations. The safety control algorithm of the AEBS is designed to secure the longitudinal safety with an environment sensor such as a radar. The control actions of the AEBS consist of warning and emergency braking. In case of the safety systems such as ESC and torque vectoring, the safety control algorithm is generally designed so that the yaw rate of the vehicle can track the desired yaw rate for securing the lateral safety. The desired yaw rate is derived based on the steady-state condition using steering input, yaw rate, and longitudinal velocity. The aforementioned systems are controlled by yaw moment control using total or differential braking. Various studies related to the lateral safety of vehicles have been conducted.

Smith *et al*. (2018) studied the effect of both passively and actively modified vehicle handling characteristics on minimum time maneuvering for a vehicle with 4-wheel torque vectoring and analyzed the effect of the target understeer gradient as the key tuning parameter. Filippis *et al*. (2018) presented the energy-efficient torque-vectoring

control algorithm for electric vehicles with multiple drivetrains through the appropriate tuning of the reference understeer characteristics. Novellis *et al*. (2014a) proposed the algorithm for the continuous and precise modulation of the driving and braking torques of each wheel for controlling the performance of a vehicle in steady-state and transient conditions. In addition, the authors presented a comparison between different torque-vectoring control structures, such as a sliding mode controller and a PID controller, for the yaw moment control (Novellis *et al*., 2014b). Siampis *et al*. (2015a) developed a model predictive control based on a constrained optimal control architecture for combined velocity, yaw, and sideslip regulation. This configuration was used for stabilization of the vehicle near the limit of lateral acceleration using the rear axle electric torque vectoring configuration of an electric vehicle. In addition, the authors also proposed a control architecture to stabilize a vehicle near the limit of lateral acceleration using the rear axle electric torque vectoring configuration (Siampis *et al*., 2015b). Kasinathan *et al*. (2016) proposed the optimal torque vectoring control algorithm for vehicle application with real-time constraints using holistic cornering control (HCC) optimization. Koehler *et al*. (2017) developed a novel torque vectoring concept for battery electric vehicles propelled by wheel individual electric machines by taking advantage of the provided degrees of freedom to reduce energy consumption. Goggia *et al*. (2015) presented an integral sliding mode formulation for the torque vectoring control of a fully electric vehicle and its performance evaluation was conducted in steady-state and transient conditions.

After careful review of the previous studies, it was found that the previous studies are generally focused on the development of current states based optimal safety control. In addition, the predictive control algorithm for safety is only based on the rear-wheels of the vehicle and does not consider physical constraints such as the limit of transmission output torque. The model predictive control is very widely used for multivariable control applications with various constraints such as equality, inequality, boundary constraints. Therefore, two types of torque vectoring for 4WD vehicles were proposed in this study, based on the model predictive control with various physical constraints. The developed two types of torque vectoring are rear-wheel and all-wheel torque vectoring algorithms. The limits of tire force, tire force change rate, and output torque from transmission were applied to the model predictive control as physical constraints. The performance evaluation of the torque vectoring algorithm proposed in this study was conducted using MATLAB/Simulink and CarSim under various evaluation scenarios such as step steering, double lane change, and circular motion. Furthermore, the evaluation results of the MPC-based torque vectoring algorithm were compared to those of the linear quadratic regulator (LQR) based torque vectoring algorithm. The main contribution of this study is to develop and evaluate the MPC-based rear and all-wheel torque vectoring algorithms by considering state prediction and driver's steering angle with the aforementioned physical constraints.

The rest of this paper is organized as follows. The second section describes the MPC-based torque vectoring algorithm. The third section presents the performance evaluation results. Finally, concluding remarks are provided in the fourth section.

2. MPC-BASED TORQUE VECTORING

The torque vectoring algorithm proposed in this study consists of three controllers, i.e., a supervisory controller, a high-level controller, and a low-level controller. Figure 1 describes the three controllers for the model predictive torque vectoring algorithm.

The desired motion of the vehicle for securing safety was computed in the supervisory controller using vehicle states. In the high-level controller, the desired longitudinal forces were derived so that the vehicle motion can track the desired motion. Based on the desired forces, torque inputs were calculated using wheel dynamics. It is assumed that the required states such as tire forces and velocities can be estimated or using various filters or mathematical techniques.

2.1. Supervisor Controller

In this study, the steady-state yaw rate was used as the desired motion to secure the lateral safety of the vehicle. The equation for steady-state value of the vehicle is given in Equation (1).

$$\dot{\psi}_{ss} = \frac{1}{\left(1 - \frac{m}{2(l_f + l_r)^2}\frac{l_f C_f - l_r C_r}{C_f C_r} v_x^2\right)} \frac{v_x}{l_f + l_r}\delta \tag{1}$$

Based on the derived steady-state yaw rate of the vehicle, the desired forces are computed using the model predictive control algorithm in the high-level controller.

2.2. High-level Controller

Figure 2 shows the detailed model schematics of the high-

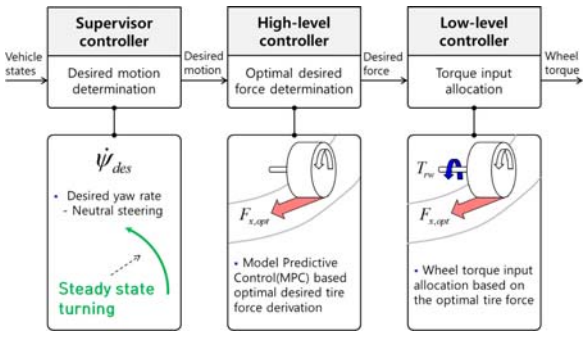

Figure 1. Three controllers for torque vectoring.

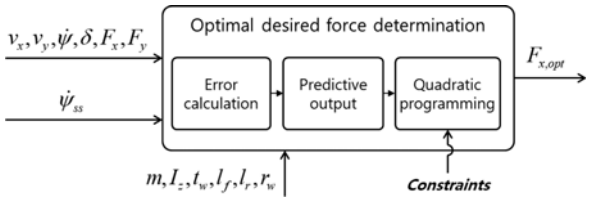

Figure 2. Detailed model schematics of the high-level controller.

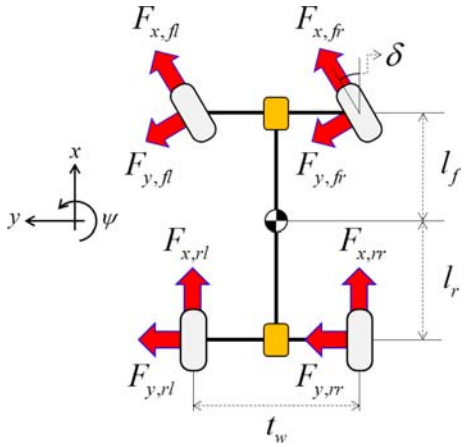

Figure 3. Free-body diagram of vehicle planar model.

level controller.

In order to compute the error and predictive output, the error dynamics derived from the vehicle planar model were used. The used planar model of the vehicle and the dynamic equations are described in Figure 3 and Equations (2) ~ (4).

$$m(\dot{v}_x - v_y\dot{\psi}) = (F_{x,fl} + F_{x,fr})\cos\delta - (F_{y,fl} + F_{y,fr})\sin\delta + F_{x,rl} + F_{x,rr} \tag{2}$$

$$m(\dot{v}_y + v_x\dot{\psi}) = (F_{x,fl} + F_{x,fr})\sin\delta + (F_{y,fl} + F_{y,fr})\cos\delta + F_{y,rl} + F_{y,rr} \tag{3}$$

$$I_z\ddot{\psi} = l_f\left[(F_{y,fl} + F_{y,fr})\cos\delta + (F_{x,fl} + F_{x,fr})\sin\delta\right] - l_r(F_{y,rl} + F_{y,rr}) + \frac{t_w}{2}\left[F_{y,fl}\sin\delta - F_{x,fl}\cos\delta - F_{x,rl}\right] + \frac{t_w}{2}\left[F_{x,fr}\cos\delta - F_{y,fr}\sin\delta + F_{x,rr}\right] \tag{4}$$

Based on the nonlinear vehicle dynamics described in the Equations (2) ~ (4), the linear error dynamics were derived using Jacobian matrices of the dynamic equations based on the error states. The defined error state is given in Equation (5).

$$e = X - X_{des} \tag{5}$$

$$X = \begin{bmatrix} v_x & v_y & \dot{\psi} \end{bmatrix}^T \tag{6}$$

$$X_{des} = \begin{bmatrix} v_{x,des} & v_{y,des} & \dot{\psi}_{des} \end{bmatrix}^T \tag{7}$$

The Jacobian matrices based error dynamics formed state-space and matrices in the equation are described as below.

$$\dot{e} = Ae + Bu + Fw \tag{8}$$

$$A = \begin{bmatrix} 0 & \dot{\psi} & v_y \\ -\dot{\psi} & 0 & v_x \\ 0 & 0 & 0 \end{bmatrix} \tag{9}$$

$$B = \begin{bmatrix} \frac{\cos\delta}{m} & \frac{\cos\delta}{m} & \frac{1}{m} & \frac{1}{m} \\ \frac{\sin\delta}{m} & \frac{\sin\delta}{m} & 0 & 0 \\ \frac{l_f\sin\delta}{I_z} - \frac{t_w\cos\delta}{2I_z} & \frac{t_w\cos\delta}{2I_z} + \frac{l_f\sin\delta}{I_z} & \frac{-t_w}{2I_z} & \frac{t_w}{2I_z} \end{bmatrix} \tag{10}$$

$$F = -X_{des} + AX_{des} + F_e w_e \tag{11}$$

$$F_e = \begin{bmatrix} F_{e,1} & F_{e,2} & F_{e,3} \end{bmatrix}^T \tag{12}$$

$$F_{e,1} = -\frac{\cos\delta(F_{y,fl} + F_{y,fr}) + \sin\delta(F_{x,fl} + F_{x,fr})}{m}$$

$$F_{e,2} = \frac{\cos\delta(F_{x,fl} + F_{x,fr}) - \sin\delta(F_{y,fl} + F_{y,fr})}{m}$$

$$F_{e,3} = \frac{l_f\left[\cos\delta(F_{x,fl} + F_{x,fr}) - \sin\delta(F_{y,fl} + F_{y,fr})\right]}{I_z} + \frac{t_w(F_{y,fl}\cos\delta + F_{x,fl}\sin\delta)}{2I_z} - \frac{t_w(F_{y,fr}\cos\delta + F_{x,fr}\sin\delta)}{2I_z}$$

where the disturbance term w in the Equation (8) represents the steering angle δ, and w_e in the Equation (11) is equal to unity. In addition, the defined input vector u is the input vector defined as $[F_{x,fl}\ F_{x,fr}\ F_{x,rl}\ F_{x,rr}]^T$. Based on the derived continuous error dynamic equation, the predictive output for quadratic programming was computed using the discretized error dynamic equation. The predictive output Y can be computed based on the following equations using the discretized error dynamic equation.

$$e(k+1) = A_d e(k) + B_d u(k) + F_d w(k) \tag{13}$$

where matrices A_d, B_d, and F_d represent the system matrix, the input matrix, and the disturbance matrix of the discretized error dynamics, respectively.

$$Y = Ge(k) + HU + Lu(k) + MW + Kw(k) \tag{14}$$

$$G = \begin{bmatrix} CA_d & CA_d^2 & \cdots & CA_d^N \end{bmatrix}^T \tag{15}$$

$$H = \begin{bmatrix} 0 & 0 & \cdots & 0 \\ CB_d & 0 & \cdots & 0 \\ \vdots & \vdots & \ddots & \vdots \\ CA_d^{N-2}B_d & CA_d^{N-3}B_d & \cdots & 0 \end{bmatrix} \tag{16}$$

$$U = \begin{bmatrix} u(k+1) & u(k+2) & \cdots & u(k+N) \end{bmatrix}^{\mathrm{T}} \tag{17}$$

$$L = \begin{bmatrix} CB_{\mathrm{d}} & C_{\mathrm{d}}A_{\mathrm{d}}B_{\mathrm{d}} & \cdots & C_{\mathrm{d}}A_{\mathrm{d}}^{\mathrm{N}-1}B_{\mathrm{d}} \end{bmatrix}^{\mathrm{T}} \tag{18}$$

$$M = \begin{bmatrix} 0 & 0 & \cdots & 0 \\ CF_{\mathrm{d}} & 0 & \cdots & 0 \\ \vdots & \vdots & \ddots & \vdots \\ CA_{\mathrm{d}}^{\mathrm{N}-2}F_{\mathrm{d}} & CA_{\mathrm{d}}^{\mathrm{N}-3}F_{\mathrm{d}} & \cdots & 0 \end{bmatrix} \tag{19}$$

$$W = \begin{bmatrix} w(k+1) & w(k+2) & \cdots & w(k+N) \end{bmatrix}^{\mathrm{T}} \tag{20}$$

$$K = \begin{bmatrix} CF_{\mathrm{d}} & CA_{\mathrm{d}}F_{\mathrm{d}} & \cdots & CA_{\mathrm{d}}^{\mathrm{N}-1}F_{\mathrm{d}} \end{bmatrix}^{\mathrm{T}} \tag{21}$$

where C is the weighting matrix for the error state vector. In order to derive the optimal desired longitudinal tire forces, the performance index J is defined as follows.

$$J = Y^{\mathrm{T}}Y + rU^{\mathrm{T}}D^{\mathrm{T}}DU \tag{22}$$

where, r and D represent the weighting factor and the difference matrix for input, respectively. By applying the computed predictive output to the equation (22), the performance index can be rewritten in quadratic form as follows.

$$J = \frac{1}{2}U^{\mathrm{T}}QU + f^{\mathrm{T}}U \tag{23}$$

$$Q = rD^{\mathrm{T}}D + H^{\mathrm{T}}H \tag{24}$$

$$f = H^{\mathrm{T}}(Ge(k) + Lu(k) + MW + Kw(k)) \tag{25}$$

The optimal input vector U can be computed using quadratic programming, and the function of QPsolver provided in MATLAB was used in this study.

In order to ensure the derivation of realistic inputs, three types of constraints, namely equality, inequality, and boundary constraints, were considered and applied to the quadratic programming. Moreover, the constraints were applied to rear-wheel torque vectoring and all-wheel torque vectoring separately in different forms. The applied constraints are described as follows.

– *In case of rear-wheel torque vectoring*

Equality constraint: $A_{\mathrm{eq,r}}U = B_{\mathrm{eq,r}}$

$$A_{\mathrm{eq,r}} = \begin{bmatrix} 1 & 0 & 0 & 0 & \cdots \\ 0 & 1 & 0 & 0 & \cdots \\ 0 & 0 & r_{\mathrm{w}} & r_{\mathrm{w}} & \cdots \\ 0 & 0 & 0 & 0 & \cdots \\ \vdots & \vdots & \vdots & \vdots & \ddots \end{bmatrix},\ size\left[(4\times N)\times(4\times N)\right] \tag{26}$$

$$B_{\mathrm{eq,r}} = \begin{bmatrix} F_{\mathrm{x,fl}}(k) & F_{\mathrm{x,fr}}(k) & B_{\mathrm{eq,r}}(3) & 0 & \cdots \end{bmatrix}^{\mathrm{T}},\ size\left[(4\times N)\times 1\right] \tag{27}$$

$$\begin{aligned} B_{\mathrm{eq,r}}(3) = {} & r_{\mathrm{f}}T_{\mathrm{trcase,r}}(k) - I_{\mathrm{w}}\dot{\omega}_{\mathrm{rl}}(k) - I_{\mathrm{w}}\dot{\omega}_{\mathrm{rr}}(k) \\ & - eF_{\mathrm{z,rl}}(k) - eF_{\mathrm{z,rr}}(k) \end{aligned} \tag{28}$$

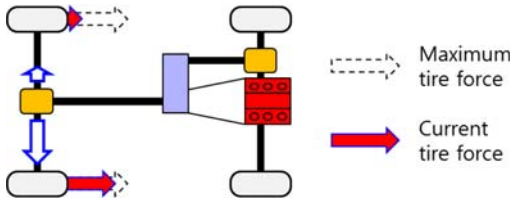

Figure 4. Concept of rear-wheel torque vectoring.

Inequality constraint: $A_{\mathrm{in,r}}U \le B_{\mathrm{in,r}}$

$$A_{\mathrm{in,r}} = \begin{bmatrix} A_{\mathrm{in,r}}(1) \\ A_{\mathrm{in,r}}(2) \end{bmatrix},\ B_{\mathrm{in,r}} = \begin{bmatrix} B_{\mathrm{in,r}}(1) \\ B_{\mathrm{in,r}}(2) \end{bmatrix} \tag{29}$$

$$A_{\mathrm{in,r}}(1) = \begin{bmatrix} 0 & 0 & 0 & 0 & 0 & 0 & 0 & 0 & \cdots \\ 0 & 0 & 0 & 0 & 0 & 0 & 0 & 0 & \cdots \\ 0 & 0 & 1 & 0 & 0 & 0 & 0 & 0 & \cdots \\ 0 & 0 & 0 & 1 & 0 & 0 & 0 & 0 & \cdots \\ 0 & 0 & 0 & 0 & 0 & 0 & 0 & 0 & \cdots \\ 0 & 0 & 0 & 0 & 0 & 0 & 0 & 0 & \cdots \\ 0 & 0 & -1 & 0 & 0 & 0 & 1 & 0 & \cdots \\ 0 & 0 & 0 & -1 & 0 & 0 & 0 & 1 & \cdots \\ \vdots & \vdots & \vdots & \vdots & \vdots & \vdots & \vdots & \vdots & \ddots \end{bmatrix} \tag{30}$$

$$A_{\mathrm{in,r}}(2) = -A_{\mathrm{in,r}}(1) \tag{31}$$

$$B_{\mathrm{in,r}}(1) = \begin{bmatrix} 0 \\ 0 \\ F_{\mathrm{x,rl}}(k) + \Delta F_{\mathrm{x,max}} \\ F_{\mathrm{x,rr}}(k) + \Delta F_{\mathrm{x,max}} \\ 0 \\ 0 \\ \Delta F_{\mathrm{x,max}} \\ \Delta F_{\mathrm{x,max}} \\ \vdots \end{bmatrix},\ B_{\mathrm{in,r}}(2) = \begin{bmatrix} 0 \\ 0 \\ -F_{\mathrm{x,rl}}(k) + \Delta F_{\mathrm{x,max}} \\ -F_{\mathrm{x,rr}}(k) + \Delta F_{\mathrm{x,max}} \\ 0 \\ 0 \\ \Delta F_{\mathrm{x,max}} \\ \Delta F_{\mathrm{x,max}} \\ \vdots \end{bmatrix} \tag{32}$$

Boundary constraint: $U_{\min} \le U \le U_{\max}$

$$U_{\min} = \begin{bmatrix} F_{\mathrm{x,fl,min}} \\ F_{\mathrm{x,fr,min}} \\ F_{\mathrm{x,rl,min}} \\ F_{\mathrm{x,rr,min}} \\ \vdots \end{bmatrix},\ U_{\max} = \begin{bmatrix} F_{\mathrm{x,fl,max}} \\ F_{\mathrm{x,fr,max}} \\ F_{\mathrm{x,rl,max}} \\ F_{\mathrm{x,rr,max}} \\ \vdots \end{bmatrix} \tag{33}$$

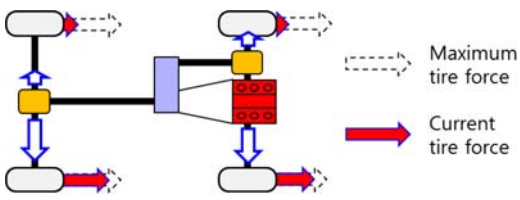

Figure 5. Concept of all-wheel torque vectoring.

– *In case of all-wheel torque vectoring*

Equality constraint: $A_{\mathrm{eq,a}}U = B_{\mathrm{eq,a}}$

$$A_{\mathrm{eq,a}} = \begin{bmatrix} r_{\mathrm{w}} & r_{\mathrm{w}} & r_{\mathrm{w}} & r_{\mathrm{w}} & \cdots \\ 0 & 0 & 0 & 0 & \cdots \\ 0 & 0 & 0 & 0 & \cdots \\ 0 & 0 & 0 & 0 & \cdots \\ \vdots & \vdots & \vdots & \vdots & \ddots \end{bmatrix},\ size\left[(4\times N)\times(4\times N)\right] \tag{34}$$

$$B_{\mathrm{eq,a}} = \begin{bmatrix} B_{\mathrm{eq,a}}(1) & 0 & 0 & 0 & \cdots \end{bmatrix}^{\mathrm{T}},\ size\left[(4\times N)\times 1\right] \tag{35}$$

$$\begin{aligned} &B_{\mathrm{eq,a}}(3) = r_{\mathrm{f}}T_{\mathrm{tr,out}}(k) - I_{\mathrm{w}}\dot{\omega}_{\mathrm{rl}}(k) - I_{\mathrm{w}}\dot{\omega}_{\mathrm{rr}}(k) \\ &-I_{\mathrm{w}}\dot{\omega}_{\mathrm{rl}}(k) - I_{\mathrm{w}}\dot{\omega}_{\mathrm{rr}}(k) - eF_{\mathrm{z,fl}}(k) - eF_{\mathrm{z,fr}}(k) \\ &-eF_{\mathrm{z,rl}}(k) - eF_{\mathrm{z,rr}}(k) \end{aligned} \tag{36}$$

Inequality constraint: $A_{\mathrm{in,a}}U \le B_{\mathrm{in,a}}$

$$A_{\mathrm{in,a}} = \begin{bmatrix} A_{\mathrm{in,a}}(1) \\ A_{\mathrm{in,a}}(2) \end{bmatrix},\ B_{\mathrm{in,a}} = \begin{bmatrix} B_{\mathrm{in,a}}(1) \\ B_{\mathrm{in,a}}(2) \end{bmatrix} \tag{37}$$

$$A_{\mathrm{in,a}}(1) = \begin{bmatrix} 1 & 0 & 0 & 0 & 0 & 0 & 0 & 0 & \cdots \\ 0 & 1 & 0 & 0 & 0 & 0 & 0 & 0 & \cdots \\ 0 & 0 & 1 & 0 & 0 & 0 & 0 & 0 & \cdots \\ 0 & 0 & 0 & 1 & 0 & 0 & 0 & 0 & \cdots \\ -1 & 0 & 0 & 0 & 1 & 0 & 0 & 0 & \cdots \\ 0 & -1 & 0 & 0 & 0 & 1 & 0 & 0 & \cdots \\ 0 & 0 & -1 & 0 & 0 & 0 & 1 & 0 & \cdots \\ 0 & 0 & 0 & -1 & 0 & 0 & 0 & 1 & \cdots \\ \vdots & \vdots & \vdots & \vdots & \vdots & \vdots & \vdots & \vdots & \ddots \end{bmatrix} \tag{38}$$

$$A_{\mathrm{in,a}}(2) = -A_{\mathrm{in,a}}(1) \tag{39}$$

$$B_{\mathrm{in,a}}(1) = \begin{bmatrix} F_{\mathrm{x,fl}}(k) + \Delta F_{\mathrm{x,max}} \\ F_{\mathrm{x,fr}}(k) + \Delta F_{\mathrm{x,max}} \\ F_{\mathrm{x,rl}}(k) + \Delta F_{\mathrm{x,max}} \\ F_{\mathrm{x,rr}}(k) + \Delta F_{\mathrm{x,max}} \\ \Delta F_{\mathrm{x,max}} \\ \Delta F_{\mathrm{x,max}} \\ \Delta F_{\mathrm{x,max}} \\ \Delta F_{\mathrm{x,max}} \\ \vdots \end{bmatrix},\ B_{\mathrm{in,a}}(2) = \begin{bmatrix} -F_{\mathrm{x,fl}}(k) + \Delta F_{\mathrm{x,max}} \\ -F_{\mathrm{x,fr}}(k) + \Delta F_{\mathrm{x,max}} \\ -F_{\mathrm{x,rl}}(k) + \Delta F_{\mathrm{x,max}} \\ -F_{\mathrm{x,rr}}(k) + \Delta F_{\mathrm{x,max}} \\ \Delta F_{\mathrm{x,max}} \\ \Delta F_{\mathrm{x,max}} \\ \Delta F_{\mathrm{x,max}} \\ \Delta F_{\mathrm{x,max}} \\ \vdots \end{bmatrix} \tag{40}$$

Boundary constraint: same as in the Equation (33)

The boundary constraints represent the longitudinal tire force limits of each wheel, and the equality constraints represent the torque limits. In case of the rear torque vectoring, the rear output torque of transfer case $T_{\mathrm{tcase,r}}$ was used to construct the equality constraint. In addition, the output torque of transmission $T_{\mathrm{tr,out}}$ was used for the equality constraint of the all-wheel torque vectoring. The inequality constraints applied to the torque vectoring in this study represent the limit of a change in longitudinal tire force. Based on the derived optimal tire forces, the desired torques that can provide the desired longitudinal forces were computed using wheel dynamic equation.

2.3. Low-level Controller

In the low-level controller, the wheel dynamic equation based desired wheel torques $T_{\mathrm{w,des}}$ were computed using the derived optimal longitudinal tire forces of the high-level controller. The desired wheel torques are given in the Equations (41) ~ (44).

$$T_{\mathrm{w,des,fl}} = I_{\mathrm{w}}\dot{\omega}_{\mathrm{fl}} + e_{\mathrm{r}}F_{\mathrm{z,fl}} + r_{\mathrm{w}}F_{\mathrm{x,des,fl}} \tag{41}$$

$$T_{\mathrm{w,des,fr}} = I_{\mathrm{w}}\dot{\omega}_{\mathrm{fr}} + e_{\mathrm{r}}F_{\mathrm{z,fr}} + r_{\mathrm{w}}F_{\mathrm{x,des,fr}} \tag{42}$$

$$T_{\mathrm{w,des,rl}} = I_{\mathrm{w}}\dot{\omega}_{\mathrm{rl}} + e_{\mathrm{r}}F_{\mathrm{z,rl}} + r_{\mathrm{w}}F_{\mathrm{x,des,rl}} \tag{43}$$

$$T_{\mathrm{w,des,rr}} = I_{\mathrm{w}}\dot{\omega}_{\mathrm{rr}} + e_{\mathrm{r}}F_{\mathrm{z,rr}} + r_{\mathrm{w}}F_{\mathrm{x,des,rr}} \tag{44}$$

where e_{r} represents the coefficient of rolling resistance. The wheel angular acceleration $\dot{\omega}$ was estimated based on the linear Kalman filter using wheel angular velocity as a measurement. The computed wheel torques from Equations (41) ~ (44) were used to control two clutches in the yaw control differential provided by CarSim. The results of the performance evaluation using MATLAB and CarSim software are described in the next section.

3. PERFORMANCE EVALUATION

The performance evaluation was conducted using MATLAB/Simulink and CarSim. Figure 6 shows the model schematics for the performance evaluation.

The torque vectoring algorithms were constructed and evaluated on Matlab/Simulink and the CarSim environment. The predictive driver model was used for reasonable performance evaluation with the vehicle model CS E-class provided by CarSim. The two scenarios, step

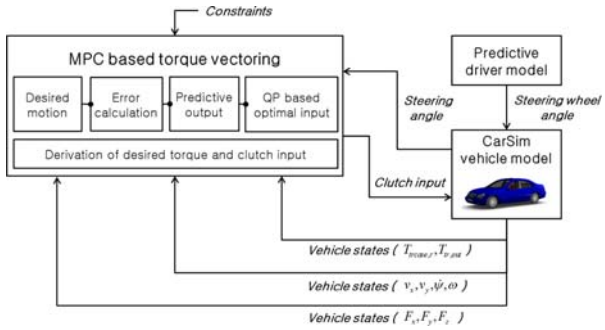

Figure 6. Model schematics for the performance evaluation.

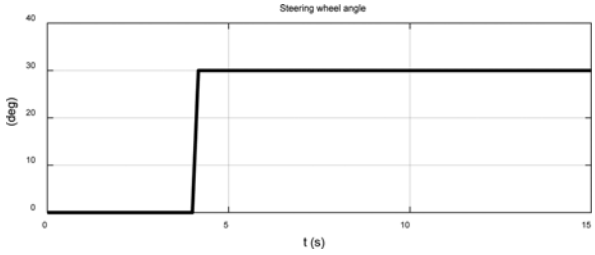

Figure 7. Result: Steering wheel angle.

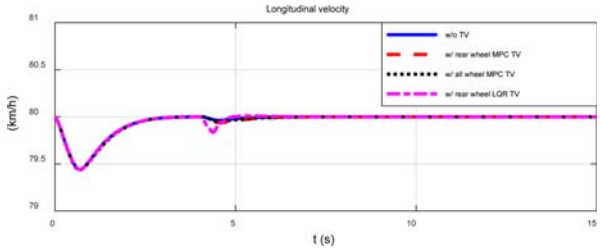

Figure 8. Result: Longitudinal velocity.

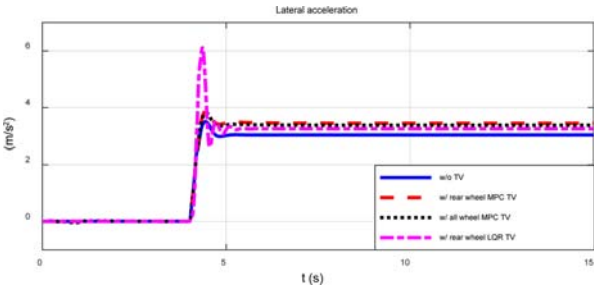

Figure 9. Result: Lateral acceleration.

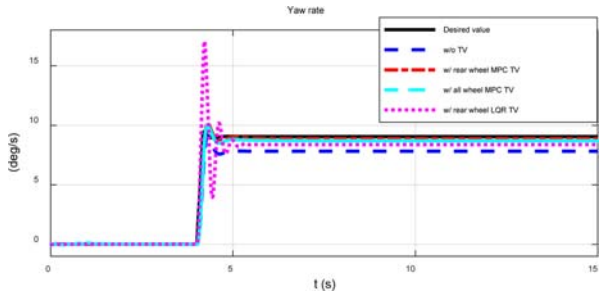

Figure 10. Result: Yaw rate (desired and current).

steering, and double lane change were used with various velocity conditions in this study. The results of the model predictive control based torque vectoring were compared to the results of the linear quadratic regulator based torque vectoring algorithm. Figures 7 ~ 18 and Table 1 show the parameters used to design of the LQR controller. The optimal feedback gains of the LQR controller have been computed based on vehicle dynamics states in every time instant. And inputs have been defined rear left and right

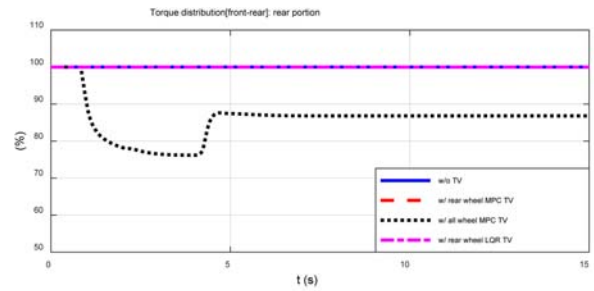

(a) Front-rear torque distribution: rear portion

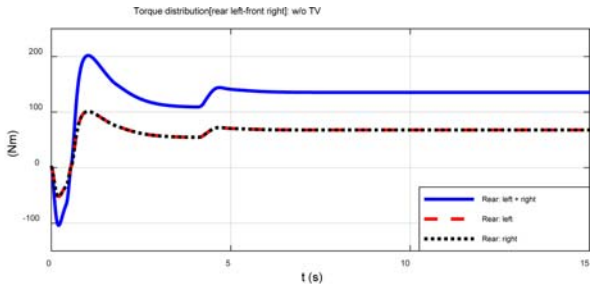

(b) Rear left-right torque: w/o TV

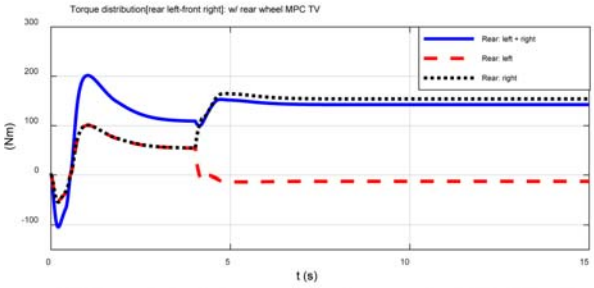

(c) Rear left-right torque: w/ rear-wheel MPC TV

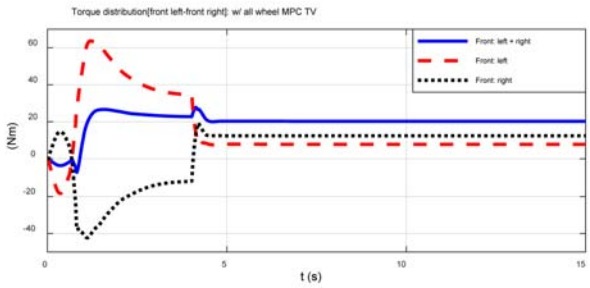

(d) Front left-right torque: w/ all-wheel MPC TV

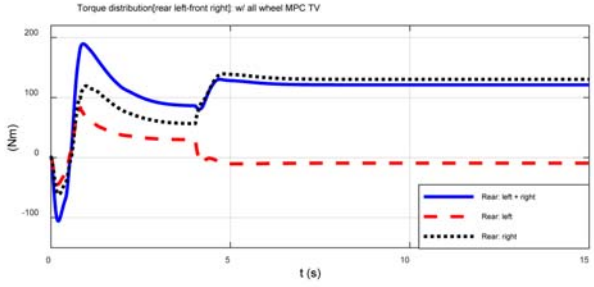

(e) Rear left-right torque: w/ all-wheel MPC TV

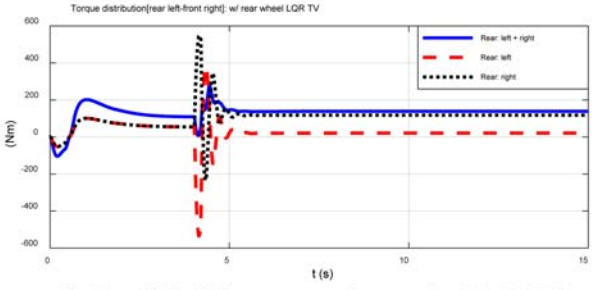

(f) Rear left-right torque: w/ rear-wheel LQR TV

Figure 11. Result: Torque distributions.

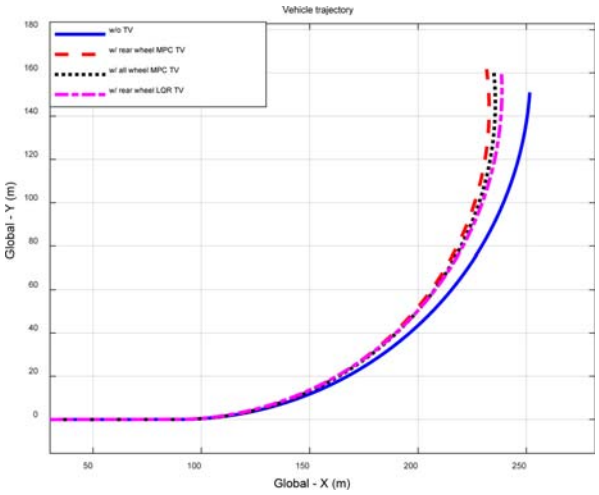

Figure 12. Result: Vehicle trajectory.

longitudinal tire forces. Table 2 shows the results and summary of the performance evaluation with respect to the chosen scenarios in this study.

As it can be seen in Figures 9 ~ 12, the results of the MPC-based torque vectoring algorithm show a sound transient response compared to the LQR based torque vectoring algorithm. In the steady-state response, all cases that use the torque vectoring algorithm show a smaller yaw rate error compared to the cases without torque vectoring. In addition, there are no significant differences in steady-state yaw rate errors of all cases that use the torque vectoring algorithm.

In case of the double lane change scenario, it can be seen that the maximum values of the steering wheel angle from

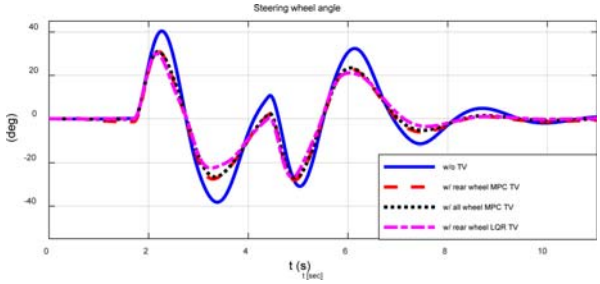

Figure 13. Result: Steering wheel angle.

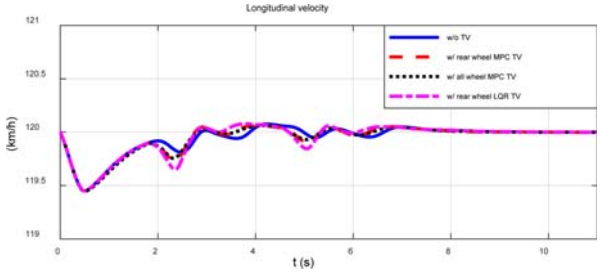

Figure 14. Result: Longitudinal velocity.

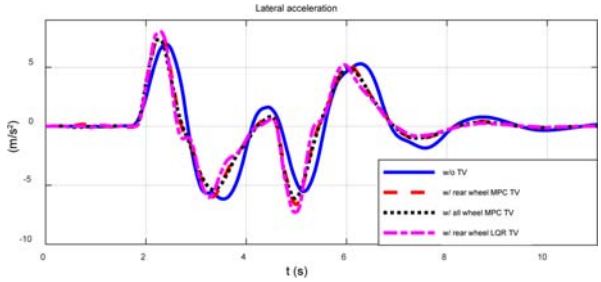

Figure 15. Result: Lateral acceleration.

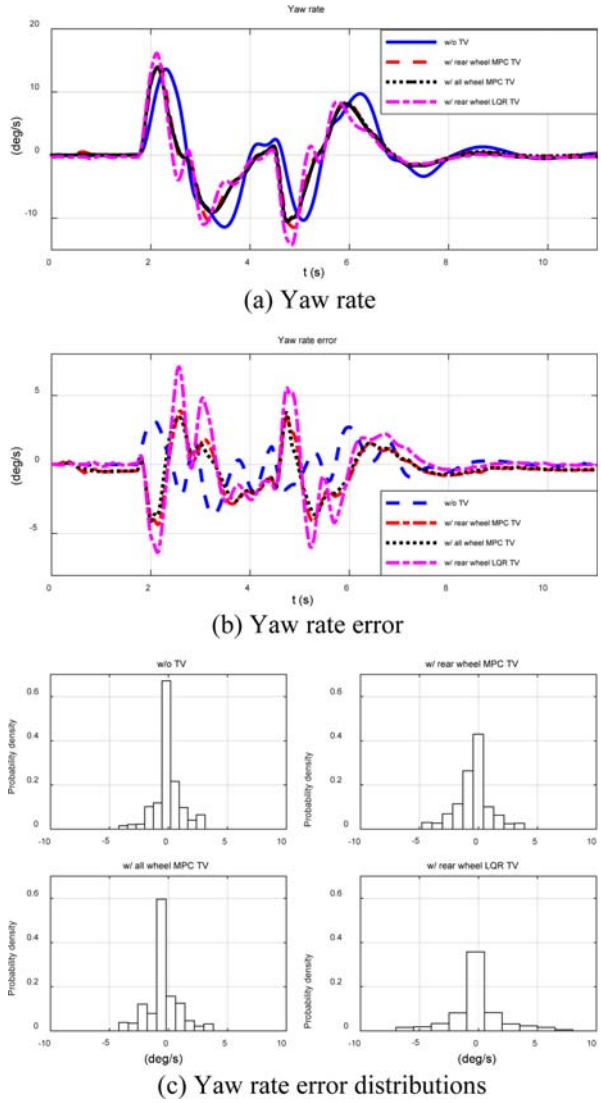

Figure 16. Result: Yaw rate (desired, current, and error).

the MPC-based torque vectoring have smaller values than those from the case without torque vectoring. However, yaw rate errors from the MPC-based torque vectoring are larger than those from the case without torque vectoring. In case of the LQR-based torque vectoring, maximum values of yaw rate and acceleration are larger than any other cases

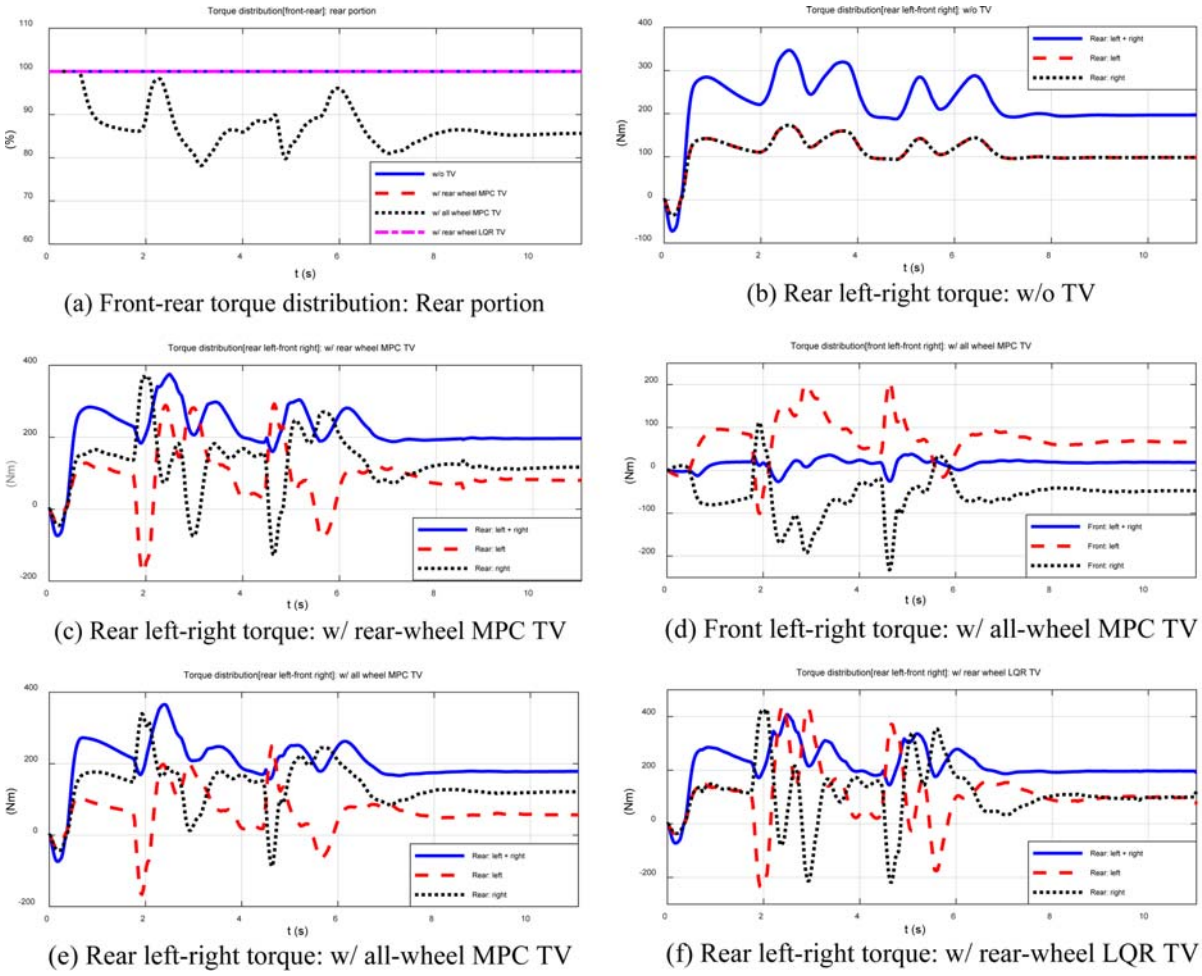

(a) Front-rear torque distribution: Rear portion

(b) Rear left-right torque: w/o TV

(c) Rear left-right torque: w/ rear-wheel MPC TV

(d) Front left-right torque: w/ all-wheel MPC TV

(e) Rear left-right torque: w/ all-wheel MPC TV

(f) Rear left-right torque: w/ rear-wheel LQR TV

Figure 17. Result: Torque distribution.

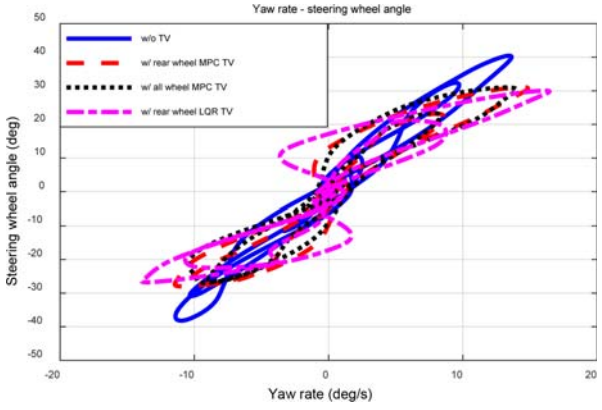

Figure 18. Result: Yaw rate – Steering wheel angle.

because the LQR controller computes optimal desired values using only current states such as velocities and forces. Based on the Figure 18, which shows the relationship between yaw rate and steering wheel angle, it is observed that the agility of the vehicle has improved by the torque vectoring algorithm. In the near zero yaw region, it is also observed that the LQR-based torque vectoring shows poor performance in comparison to the MPC-based torque vectoring case because the MPC computes optimal desired inputs by considering predictive states and driver's steering wheel angle. The concluding remarks are provided in the next section.

Table 1. Used parameters for LQR controller.

Division		Value	Remark
Weighting factors	State	diag[0 0 10,000]	Constant (v_x, v_y, yaw rate)
	Input	diag[1 1]	Constant (rear-left/right forces)
Feedback optimal gain		Time varying	Dependent on vehicle dynamic states

4. CONCLUSION

The physical constraint based model predictive rear-wheel and all-wheel torque vectoring algorithms for 4WD

Table 2. Summary of the evaluation results.

Division (unit: deg, deg/s, deg/s^2)		Yaw rate (Max)	Yaw accel (Max)	Yaw rate error (Max)	Yaw rate error (RMS)	Steering wheel angle (Max)
Step steering	w/o TV	9.11	0.96	3.61	1.08	N/A
	w/ rear MPC	10.16	1.06	2.86	0.29	N/A
	w/ all MPC	9.98	1.05	3.00	0.35	N/A
	w/ rear LQR	17.08	2.10	8.25	0.91	N/A
Double lane change	w/o TV	13.62	1.03	3.62	1.14	40.42
	w/ rear MPC	14.84	1.15	4.34	1.51	31.07
	w/ all MPC	13.97	1.23	4.11	1.40	30.98
	w/ rear LQR	16.43	1.33	7.06	2.16	30.02

vehicles were developed and evaluated in this study. The planar vehicle model was used to construct the model predictive control algorithm with physical constraints. The three types of physical constraints were the limit of tire force, the limit of tire force change rate, and the torque limit. The performance evaluation of the torque vectoring algorithm was conducted under the evaluation scenarios of step steering and double lane change on Matlab/Simulink and CarSim environments. The evaluation results of the developed algorithm were compared to the evaluation results of the linear quadratic regulator based torque vectoring algorithm. In general, the evaluation results show that the model predictive control based torque vectoring algorithm has relatively small errors between desired yaw rate and current yaw rate, compared to the linear quadratic regulator based torque vectoring. Moreover, the dynamic behaviors in the transient region of the developed algorithm show sound results compared to the linear quadratic regulator based torque vectoring algorithm. The evaluated results from the MPC-based torque vectoring showed better dynamic performances in the transient response region than those of the LQR based torque vectoring. In addition, the yaw rate errors from the cases that use torque vectoring have smaller values than those from the cases without torque vectoring. However, there are some limitations on the problems of state estimation, efficiency, and dynamic behavior. In this study, it was assumed that all states of the vehicle such as tire forces and velocities could be obtained by various estimation methods. In addition, the efficiency of torque vectoring system was not considered because the algorithm was designed to be always activated while driving. The driver's input for the longitudinal dynamic behaviors of the vehicles was also not considered in torque vectoring. Furthermore, predictive torque vectoring algorithm needs relatively a lot of time computing optimal desired inputs because of states and many physical constraints in this stage. In order for practicality and real-time capability, the development of the estimation algorithms of tire forces and velocities of vehicles is considered as future work. And conducting a feasibility study on real-time capability of the predictive torque vectoring algorithm in embedded devices based on various efficient convex optimization methods is also considered as a future work. In addition, the design of a decision algorithm to select the optimal intervention timing of the torque vectoring and control algorithm for dynamic behaviors using driver's input are also considered as future work. Nevertheless, it is expected that the model predictive torque vectoring algorithm developed in this study can be used as a safety control algorithm for 4WD vehicles.

ACKNOWLEDGEMENT–This work was supported by a research grant from Hyundai Motor Group "Future Technology Research in the year of 2017".

REFERENCES

Filippis, G. D., Lenzo, B., Sorniotti, A., Gruber, P. and Nijs, W. D. (2018). Energy-efficient torque-vectoring control of electric vehicles with multiple drivetrains. *IEEE Trans. Vehicular Technology* **67**, **6**, 4702–4715.

Goggia, T., Sorniotti, A., Novellis, L. D., Ferrara, A., Gruber, P., Theunissen, J., Steenbeke, D., Knauder, B. and Zehetner, J. (2015). Integral sliding mode for the torque-vectoring control of fully electric vehicles: Theoretical design and experimental assessment. *IEEE Trans. Vehicular Technology* **64**, **5**, 1701–1715.

Kasinathan, D., Kasaiezadeh, A., Wong, A., Khajepour, A., Chen, S. K. and Litkouhi, B. (2016). An optimal torque vectoring control for vehicle applications via real-time constraints. *IEEE Trans. Vehicular Technology* **65**, **6**, 4368–4378.

Koehler, S., Viehl, A., Bringmann, O. and Rosenstiel, W. (2017). Energy-efficiency optimization of torque vectoring control for battery electric vehicles. *IEEE Intelligent Transportation Systems Magazine* **9**, **3**, 59–74.

Novellis, L. D., Sorniotti, A. and Gruber, P. (2014a). Wheel torque distribution criteria for electric vehicles with torque-vectoring differentials. *IEEE Trans. Vehicular Technology* **63**, **4**, 1593–1602.

Novellis, L. D., Sorniotti, A., Gruber, P. and Pennycott, A. (2014b). Comparison of feedback control techniques for torque-vectoring control of fully electric vehicles. *IEEE Trans. Vehicular Technology* **63**, **8**, 3612–3623.

Siampis, E., Velenis, E. and Longo, S. (2015a). Rear-wheel torque vectoring model predictive control with velocity

regulation for electric vehicles. *Int. J. Vehicle Mechanics and Mobility* **53**, **11**, 1555–1579.

Siampis, E., Velenis, E. and Longo, S. (2015b). Model Predictive torque vectoring control for electric vehicles near the limits of handling. *Proc. European Control Conf. (ECC)*, Linz, Austria.

Smith, E. N., Velenis, E., Tavernini, D. and Cao, D. (2018). Effect of handling characteristics on minimum time cornering with torque vectoring. *Int. J. Vehicle Mechanics and Mobility* **56**, **2**, 221–248.